EUROMECH COLLOQUIUM 578
Rolling Contact Mechanics for Multibody System Dynamics
Funchal, Madeira, Portugal, April 10 to 13, 2017
J.Ambrósio, W.Schiehlen, J.Pombo (Editors)

AN ADVANCED MODELING TECHNIQUE FOR ROLLING ELEMENT BEARINGS IN ELASTOHYDRODYNAMIC (EHL) FIELD

Leoluca Scurria*, Jakob Fiszer†, Tommaso Tamarozzi*†, Pavel Jiranek*, Wim Desmet†

*Siemens Industry Software NV
Interleuvenlaan 68, 3001, Leuven, Belgium
leoluca.scurria@siemens.com, tommaso.tamarozzi@siemens.com

†KU Leuven
Celestijnenlaan 300B, 3001 Leuven, Belgium

Keywords: Bearing Elastohydrodynamic Lubrication, EHL, Modeling Technique, Multibody, Analytical Model.

Summary: *The large use of rolling element bearings in power transmissions, together with the constantly growing request for computationally efficient and accurate predictions of their system-level NVH performances, is pushing the development of novel numerically efficient modeling techniques. FE-based approaches turn out to be too time consuming for system-level machine analysis. For this purpose the attention is often focused on analytical models that are able to grasp the essential effects characterizing the solution while guaranteeing fast and reliable results. The conducted research presented in this paper takes a step forwards by proposing a bearing modeling strategy that is able to simulate the bearing behavior while accounting for the most relevant phenomena such as EHL, centrifugal loads, roller crowning and roller-raceway misalignment. The strategy has been developed for angular contact ball bearings and roller bearings but it can be easily extended to other cases (e.g. deep groove and thrust ball bearings, tapered and barrel roller bearings). The proposed modeling techniques consider 5-dof (degrees of freedom) inner ring displacement with respect to the outer ring together with their relative rotational speed. The output is thus given by the 5-dof reaction forces and moments acting on the bearing's shaft due to the displacement vector assigned as input. The strategy consists of three steps. Starting from the input vector, the first step is to compute the relative displacement of the rings for each rolling element location. Then the EHL contact model is introduced to compute the rolling element equilibrium by imposing force equilibrium. Once the equilibrium of each rolling element is computed, a kinematics-based transformation matrix is applied to each contact force giving the equivalent forces and moments with respect to the bearing axis. Finally, each rolling element contribution with respect to the bearing axis is summed defining the output vector.*

1. INTRODUCTION

The evaluation of the behavior of a rolling element bearing is in general a nonlinear, statically indeterminate problem.

A systematic approach for the solution of deep groove, angular contact ball bearings and tapered roller bearings has been presented by Andreason [1, 2] in which vectors are introduced to describe the geometry, displacements and forces. The analysis of Andreason has been extended by Liu[3] to consider high speed effects of roller centrifugal loads and gyroscopic moment.

The approach proposed in this work starts from the contact modeling and rolling element behavior to describe the complete bearing behavior in EHL field while accounting for centrifugal loads, roller crowning and roller-raceway misalignment.

The solution for EHL point contacts has been tackled with numerical methods, starting from Newton Raphson algorithms (e.g. Hamrock and Dowson [4]) and then introducing more sophisticated methods such as the multigrid technique (e.g. Brandt and Livne [5]). Thereafter Wijnant [6] has adopted these numerical models and applied curve fitting techniques on the solution in order to develop formulations which describe the steady state and transient lubricated contact behavior.

Concerning EHL line contact, through the years the Hertzian-based solution has been replaced with EHL solutions in order to improve the reliability of the models. Several formulas have been developed to predict the fluid film thickness of line contacts under steady-state conditions by Moes [7], Gelink and Schipper [8], or even in transient conditions by Sasaki et al. [9].

This work extends the work of de Mul et al. [10] by merging the presented bearing modeling technique with the aforementioned EHL contact models.

2. BALL BEARING MODEL DESCRIPTION

The model hereafter described considers as input the 5-dof inner ring displacement and shaft speed with respect to the outer ring. The model assumes steady-state conditions. The contact is considered as fully flooded and the rolling elements as pure rolling onto the raceways.

Due to the steady state hypothesis the time dependent solution of the rolling elements will not be taken into account, thus phenomena such as the rolling element bouncing between the raceways is not considered. The centrifugal force is introduced as a force exerting on the center of gravity of the rolling element.

Contact friction is neglected as well, hence the rotation around the bearing axis is not considered as a dof. The output of the model will be the 5-dof reaction forces and moment exerting on the bearing axis.

The model description starts from the definition of the coordinate system used and the transformations needed to describe quantities on the two different levels, respectively bearing and rolling element. Similar to what has been done by de Mul et al. [10] two coordinate systems will be placed: the global coordinates system to describe the bearing and a second one so called local to describe the single rolling element behavior. Referring to the local axis system, the

rolling element equilibrium will be computed based on the contact model proposed by Wijnant [6].

Figure 1 shows the above-mentioned coordinate systems where:

- $\{S_g\} = \{O_g; x_g, y_g, z_g\}$ is the global coordinate system where the z_g-axis corresponds to the bearing axis and O_g to the center of the bearing.
- $\{S_l\} = \{O_l; x_l, y_l, z_l\}$ where $O_l \equiv O_i$ is the inner raceway groove curvature center as shown in Figure 2, the x_l-axis is aligned with the contact force between the rolling element and the inner raceway.

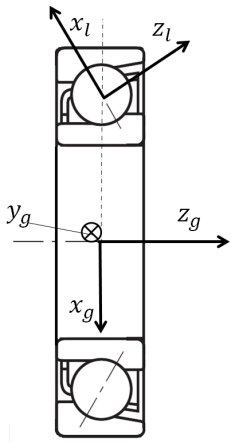

Figure 1. The global and the local coordinate system.

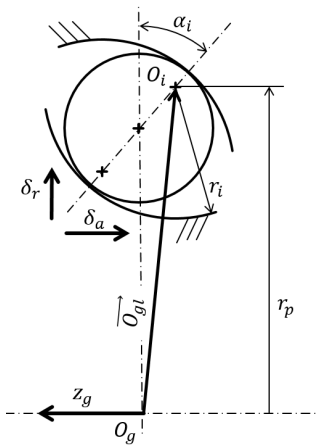

Figure 2. Cross-section geometry.

2.1 From global to local displacement

The inner ring is displaced by three translations and two rotations. These displacements are given with respect to the global coordinate system $x_g - y_g - z_g$ shown in Figure 1. The translations along the three axes are named respectively δ_x, δ_y and δ_z. The rotation around the axes x_g and y_g will be respectively γ_x and γ_y. Once the inner ring is displaced, it will displace locally in each rolling element location. This displacement will cause the rolling element to be squeezed between the raceways. The local displacement of the inner ring with respect to a nominal configuration can be defined by the parameters δ_a and δ_r which are respectively the axial and the radial displacement shown in Figure 2. The local inner ring displacement depends on the rolling element position. The position of the cross section plane related to each rolling element can be defined introducing the angle ψ shown in Figure 3. In order to calculate the local inner ring displacement for a given global inner ring displacement, one must introduce the vector $\overrightarrow{\boldsymbol{O}_{gl}}$ which goes from O_g to O_l.

$\overrightarrow{\boldsymbol{O}_{gl}}$ written in global coordinates reads:

$$\overrightarrow{\boldsymbol{O}_{gl}} = \left[r_p \cos\psi \quad r_p \sin\psi \quad (r_i - D/2)\cos\alpha_i\right]^T. \tag{1}$$

Where $(r_i - D/2)\cos\alpha$ is also referred to as z_{ref}. Now the axial and radial local inner ring displacement associated to the global displacement can be written as:

$$\delta_a = -\delta_z - \begin{bmatrix}\gamma_x & \gamma_y & 0\end{bmatrix}^T \times \begin{bmatrix}r_p\cos\psi & r_p\sin\psi & 0\end{bmatrix}^T, \tag{2}$$

$$\delta_r = \begin{bmatrix}\cos\psi & \sin\psi & 0 & -z_{ref}\sin\psi & z_{ref}\cos\psi\end{bmatrix}\begin{bmatrix}\delta_x & \delta_y & \delta_z & \gamma_x & \gamma_y\end{bmatrix}^T. \tag{3}$$

Where the minus sign in (2) is due to the opposite direction between z_g and the positive direction of δ_a (See Figure 2)

2.2 Procedure to compute contact loads in global coordinates

Once the local inner ring displacement at each ball location is computed, the equilibrium of the rolling element will be calculated (see 2.3). It returns the contact loads and contact angles between the rolling element and both raceways. The contact force acting on the inner ring will have then to be referred at the global coordinate system in order to sum the contribution of each ball to achieve the complete bearing reaction forces and moments. To do so a transformation matrix has to be built which transforms a general vector of forces and moments (also called wrench vector) ${}^l\boldsymbol{w}_j$ in local coordinate system to an equivalent vector ${}^g\boldsymbol{w}_j$ in global coordinates. Where the notation states the coordinate system the wrench is expressed in and the rolling element it refers to, respectively the superscript and the subscript. For instance the local wrench vector of the j-th rolling element will be composed as follows:

$${}^l\boldsymbol{w}_j = \begin{bmatrix}{}^lF_x & {}^lF_y & {}^lF_z & {}^lM_x & {}^lM_y & {}^lM_z\end{bmatrix}. \tag{4}$$

Where ${}^lF_i$ and ${}^lM_i$ are respectively the force and the moment exerting along the i-direction in local coordinates. The first step of the procedure is to define a series of rotations which allow to align the local coordinate system with global one. Naming $\{S_g\}$, $\{S_1\}$, $\{S_l\}$ The coordinate system shown in Figure 3 and Figure 4, the transformation steps are:

- $\{S_g\} \rightarrow \{S_1\}$ The purpose of the first rotation is to align the global x-axis with the ball center as shown in Figure 3, it can be done rotating to an angle ψ around the z_g axis;
- $\{S_1\} \rightarrow \{S_l\}$ This transformation aligns the x_l axis with the line connecting the ball-inner raceway contact point and the inner ring groove center as shown in Figure 4. This rotation is done rotating by an angle α_i (ball-inner raceway contact angle in displaced configuration) around the y_1 axis.

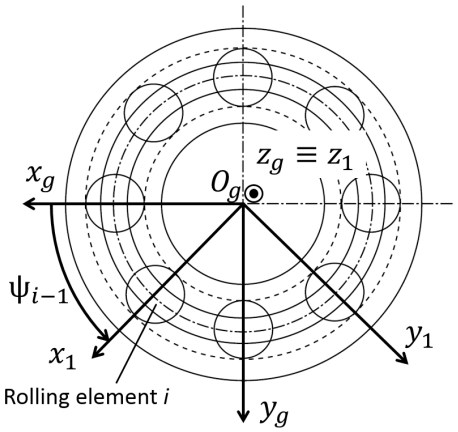

Figure 3. $\{S_g\} \rightarrow \{S_1\}$ rotation

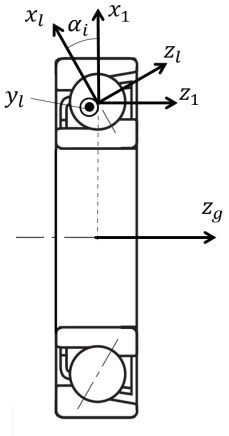

Figure 4. $\{S_1\} \rightarrow \{S_l\}$ rotation

The first ($\{S_g\} \rightarrow \{S_1\}$) and the second ($\{S_1\} \rightarrow \{S_l\}$) rotation matrices can be written as:

$$\mathbf{R}_{g1} = \begin{bmatrix} \cos\psi & -\sin\psi & 0 \\ \sin\psi & \cos\psi & 0 \\ 0 & 0 & 1 \end{bmatrix}, \qquad \mathbf{R}_{1l} = \begin{bmatrix} \cos\alpha_i & 0 & \sin\alpha_i \\ 0 & 1 & 0 \\ -\sin\alpha_i & 0 & \cos\alpha_i \end{bmatrix}. \tag{5}$$

Since the rotations are given in local axes, the transformation $\{S_g\} \rightarrow \{S_l\}$ has to be composed from left hand side to right as follows:

$$\mathbf{R}_{gl} = \mathbf{R}_{g1} \cdot \mathbf{R}_{1l} = \begin{bmatrix} \cos\psi\,\cos\alpha_i & -\sin\psi & \cos\psi\,\sin\alpha_i \\ \sin\psi\,\cos\alpha_i & \cos\psi & \sin\psi\,\sin\alpha_i \\ -\sin\alpha_i & 0 & \cos\alpha_i \end{bmatrix}. \tag{6}$$

Since the coordinate systems are also translated with respect to each other, the vector $\overrightarrow{O_{gl}}$ must be accounted for. It can be done by the introduction of the cross-product matrix $\widehat{\mathbf{O}_{gl}}$ which reads:

$$\widehat{\mathbf{O}_{gl}} = \begin{bmatrix} 0 & -O_{gl_z} & O_{gl_y} \\ O_{gl_z} & 0 & -O_{gl_x} \\ -O_{gl_y} & O_{gl_x} & 0 \end{bmatrix}. \tag{7}$$

The cross-product matrix $\widehat{\mathbf{O}_{gl}}$ is used to represent the cross product as matrix multiplication (e.g. $\overrightarrow{O_{gl}} \times \boldsymbol{b} = \widehat{\mathbf{O}_{gl}}\,\boldsymbol{b}$ where $\boldsymbol{b}$ is a vector).

Now the wrench transformation matrix can be defined, which is able to change the coordinate system and the application point of the wrench vector.

$$\mathbf{W}_{gl} = \begin{bmatrix} \mathbf{I}_{3\times3} & \mathbf{0}_{3\times3} \\ \widehat{\mathbf{O}_{gl}} & \mathbf{I}_{3\times3} \end{bmatrix} \begin{bmatrix} \mathbf{R}_{gl} & \mathbf{0}_{3\times3} \\ \mathbf{0}_{3\times3} & \mathbf{R}_{gl} \end{bmatrix}. \tag{8}$$

Where $\mathbf{0}_{3\times3}$ and $\mathbf{I}_{3\times3}$ state respectively the 3 by 3 null matrix and the 3 by 3 identity matrix.

The contribution of the j-th rolling element in global coordinates can be easily written as ${}^{g}\boldsymbol{w}_j = \mathbf{W}_{gl} \cdot^{l} \boldsymbol{w}_j$. Then the total reaction forces and moments (${}^{g}\boldsymbol{w}_{tot}$) exerting on the bearing axis can be computed as:

$$ {}^{g}\boldsymbol{w}_{tot} = \sum_{j} {}^{g}\boldsymbol{w}_j. \tag{9} $$

This method will be used to combine the effects of the rolling elements in all the developed models, both for ball as well as roller bearings. Concerning roller bearings, minor corrections are needed due to their geometry.

2.3 Rolling element equilibrium in EHL field

In this paper contact friction is neglected, because of this the contact force exerting on the raceways has to be radially oriented to the rolling element center as well as to the raceway groove curvature center. As explained by de Mul [10] in case the centrifugal load is neglected the contact forces lie on the same ball diameter (see Figure 5). When the centrifugal load is introduced, the rolling element equilibrium loses his symmetry, hence the contact angles will not be equivalent anymore. In particular the contact angle on the outer raceway becomes smaller while the one on the inner raceway bigger. Figure 6 shows the loss of symmetry and the different contact angles.

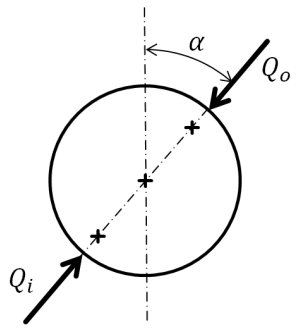

Figure 5. Rolling element equilibrium neglecting the centrifugal load.

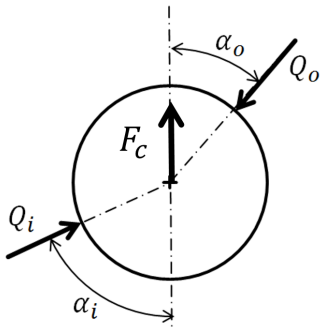

Figure 6. Loss of symmetry in rolling element equilibrium.

The centrifugal force F_c is due to the revolution of the ball around the bearing axis. Referring to Figure 6 the rolling element equilibrium can be written as:

$$ \begin{cases} F_r = Q_i cos\alpha_i - Q_o cos\alpha_o + F_c & = 0 \\ F_a = Q_i sin\alpha_i - Q_o sin\alpha_o & = 0 \end{cases} \tag{10} $$

Where the quantities Q_i, Q_o, α_i and α_o are function of the ball center displacement.
To compute the equilibrium one must solve the set of non linear equations with the ball center

displacement as unknown (See [10]). Defining $\mathbf{f} = [F_r,\ F_a]^T$ as the vector of the residuals in each iteration step, the unknown vector is consequently defined as $\boldsymbol{v} = [v_r,\ v_a]^T$. Where v_r and v_a represent respectively the radial and the axial displacement of the center of the ball with respect to the nominal configuration. To solve Eq. (10) the Newton-Raphson method can be introduced, which gives the well known iterative process $\boldsymbol{v}_{k+1} = \boldsymbol{v}_k - \mathbf{J}_k^{-1}\mathbf{f}_k$, where $\mathbf{J}_k$ is the Jacobian matrix for the *k-th* iteration step of $\mathbf{f}_k$ with respect to $\boldsymbol{v}_k$. The parameters and the procedure to describe and solve the equilibrium can be found in [10].

In order to compute the rolling element equilibrium a contact model must be introduced. Since almost any rolling element bearing works in lubricated conditions, the contact model should describe the phenomena occurring when a non-conformal contact operates in presence of lubricant. Due to the relative motion of the surfaces, the lubricant creates a thin layer which separates them. In the majority of applications this cause a pressure distribution which is so high that both the bodies deformation and the piezoviscosity of the lubricant cannot be neglected, hence EHL.

The introduction of the EHL regime typically brings more accuracy even if it turns into a computationally more expensive model. It must be underlined that, in this particular case in which steady-state and fully flooded conditions are considered, beside the more demanding computations, the introduction of the lubricated regime brings more stability to the solution process. In case of dry contact no force is defined if the surfaces are not contacting, this in turns leads to a non-smooth behavior and bad-conditioned Jacobian matrices. By the introduction of lubrication, a contact force is always defined even if extremely small. This gives a desirable smooth behavior to the iterative process.

The contact model employed in this work has been developed by Wijnant [6] where an analytic formula has been obtained which gives the bodies penetration as a function of the load exerting on the bodies. The penetration δ is defined as the penetration the undeformed surfaces would have in displaced configuration. The penetration between the rolling element and the inner and outer raceway, respectively δ_i and δ_o are defined by the center position of the ball $\boldsymbol{v}$.

Since the model developed by Wijnant is implicit, to calculate the load associated to a given penetration an iterative process must be employed (e.g. any Newton based method might serve the purpose). This means that the solution process of the rolling element equilibrium requires three iterative processes. A higher-level process which iterates the rolling element position to satisfy Eq. (10). Once $\boldsymbol{v}$ is defined for a specific iterative step, it is used to define the corresponding penetration between the rolling element and the raceways. By the penetration two parallel lower-level iterative processes calculate the load corresponding to the given penetration. And then by the contact loads the process starts again from Eq. (10) until the tolerance is satisfied.

2.4 Angular contact ball bearing solution and results

Thereafter, the previous sections are combined to achieve a procedure to compute the results for a certain bearing geometry which is defined in Table 1.

A certain angular velocity is given to the shaft, hence to the inner ring, about its main

r_i	$3.07\ mm$	Inner-ring curvature radius
r_o	$3.24\ mm$	Outer-ring curvature radius
D	$6\ mm$	Ball diameter
r_p	$15.7\ mm$	Radius of the inner raceway groove center
r_q	$15.56\ mm$	Radius of the outer raceway groove center
$clnc$	$0.0335\ mm$	Axial clearance
α	$40°$	Nominal contact angle
r_{pw}	$15.63\ mm$	Pitch radius
Z	8	Number of rolling elements
E	$206\ GPa$	Young modulus
ν	0.3	Poisson ratio
ρ	$7.8\ kg/dm^3$	Material density
α_{barus}	$1 \cdot 10^{-8}\ Pa^{-1}$	Lubricant pressure-viscosity coefficient
η_0	$0.1\ Pas$	Lubricant viscosity at ambient pressure

Table 1. Geometrical and material proprieties of the test bearing

rotational axis. The rotation of the inner ring induces a cage rotation, such that the position of the rolling elements changes during the simulation. Thus the solution is computed for a given inner ring displacement and different rotational speeds of the shaft, while the angular rotation of the shaft is kept as variable.

Figure 7 shows a qualitative flowchart of the solution process, where the blocks computing the contact solutions contain an iterative process themselves.

A case study has been computed with the following input:

$$\begin{bmatrix}\delta_x & \delta_y & \delta_z & \gamma_x & \gamma_y\end{bmatrix} = \begin{bmatrix}-2.5 \cdot 10^{-2} mm & -2.5 \cdot 10^{-2} mm & -2.5 \cdot 10^{-2}\ mm & 0.02° & 0.01°\end{bmatrix}. \quad (11)$$

The values of (11) are chosen within a range that gives reasonable values of the reaction forces and moments. Results are shown in Figure 8. Figure 8-(f) shows the equivalent contact angle of the bearing, which varies significantly as the shaft rotates. It is calculated by the axial and the radial reaction forces.

By this results is clear how the rotational speed of the shaft plays a key-role in defining the bearing stiffness. It introduces two different phenomena, the first is addressed to the centrifugal load affecting the contact angles, while the second one which is predominant is the effect on the lubricated contact. In fact as the speed of the surfaces increases, more lubricant comes in between the surfaces, hence greater fluid film thickness, hence more deformation of the solid bodies which increases the contact force.

The modulation of the reaction forces, moments and equivalent contact angle is because of the rolling elements rotating around the main axis of the bearing. The frequency of this oscillatory behavior is strictly related to the number of rolling elements and their motion around the global z-axis.

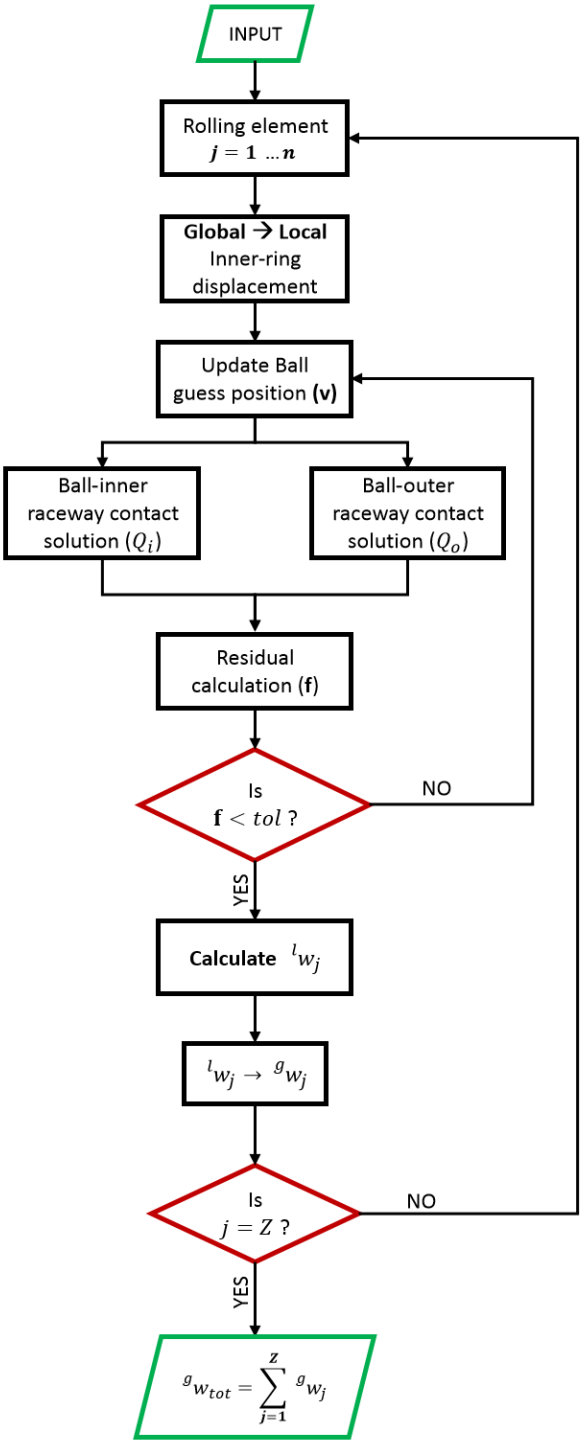

Figure 7. Qualitative flowchart of the solution process.

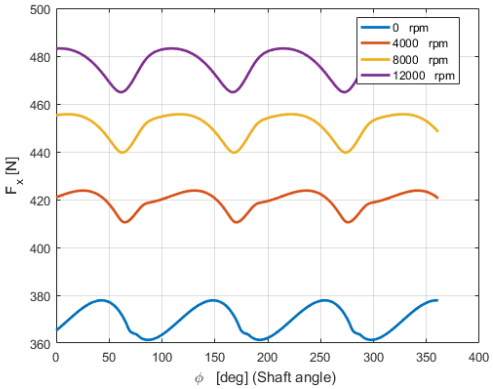

(a) Bearing reaction force along the x-axis

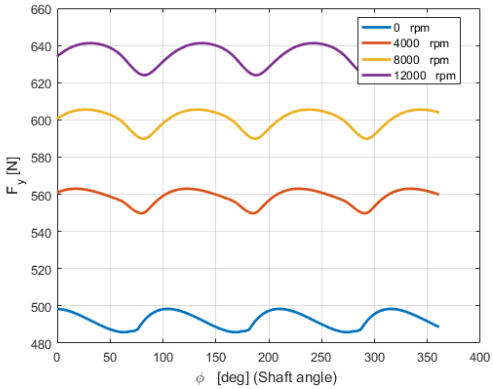

(b) Bearing reaction force along the y-axis

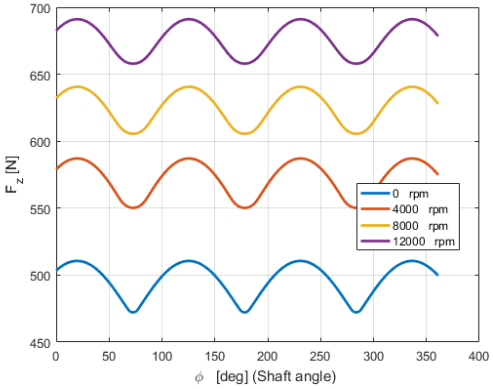

(c) Bearing reaction force along the z-axis

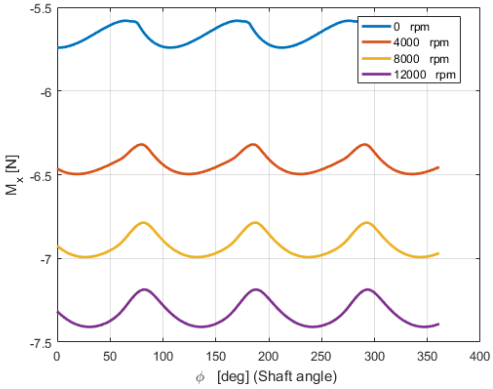

(d) Bearing reaction moment along the x-axis

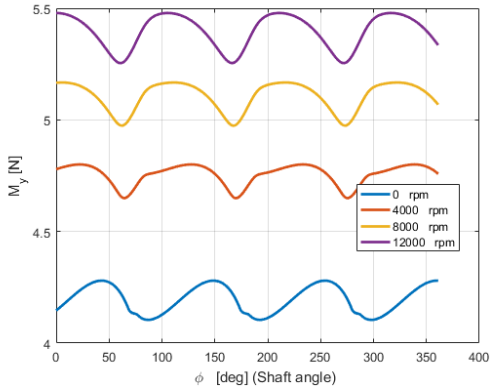

(e) Bearing reaction moment along the y-axis

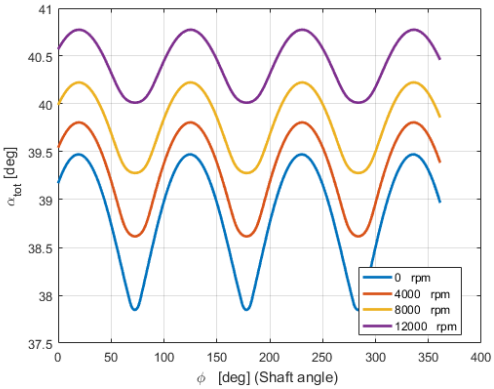

(f) Equivalent bearing angle α_{tot}

Figure 8. ACBB (Angular contact ball bearings) reaction forces and moments assuming EHL contact.

This model can be compared with the dry one. The dry model is based on the Hertz theory for elliptical contacts and has been largely explained in [11]. Figure 9 shows the comparison of the reaction force along the x-axis using two different contact models, respectively the one develped by Wijnant and the Hertz theory.

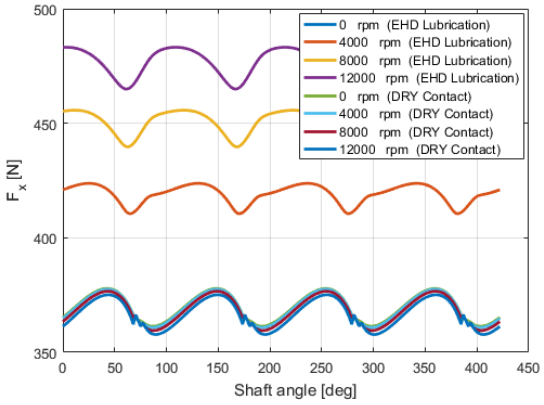

Figure 9. Comparison of the reaction force F_x calculated using EHL or Dry contact model.

The two different models return the same results in case the shaft speed is null, while the difference becomes bigger as the shaft speed increases. In fact, in case of dry contact, the shaft speed only induces the loss of symmetry in the rolling element equilibrium (see Figure 6), while in case of EHL contact model it affects the contact stiffness as well.

3. CYLINDRICAL ROLLER BEARING'S MODEL DESCRIPTION

The case of the cylindrical roller bearing is largely more complex than its ball bearing counterpart. This is mostly due to the fact that the roller-raceway contact is now considered to involve a line as opposed to the simple point contact case. The misalignment of the surfaces might here play a much larger role and techniques that allow to take this into account need to be implemented.

As done for angular contact ball bearings, and without loss of generality, the outer raceway is considered fixed in space while the inner one is displaced. The local inner raceway movement can be defined by two parameters, s_i and θ_i, where the first one is the translation approach perpendicular to the roller axis and the second one is the inner raceway rotation on the cross section plane as shown in Figure 10. To develop the model some important assumptions are done. The model will not account for roller skewing and friction. Beside this, the effects of raceways shoulders and flanges are considered negligible. Moreover the model considers steady-state conditions hence it does not account for impacts. Is assumed that stress concentrations and lubricant leaking at roller sides do not influence the solution and that the Hertz hypothesis apply.

Figure 11 shows the local coordinate system $x_l - y_l - z_l$ together with the motions of the rolling element s_x and θ_y. The parameter cl indicates the value of the radial clearance as the

maximum radial play the bearing has. The global coordinate system is the same as defined for ACBB.

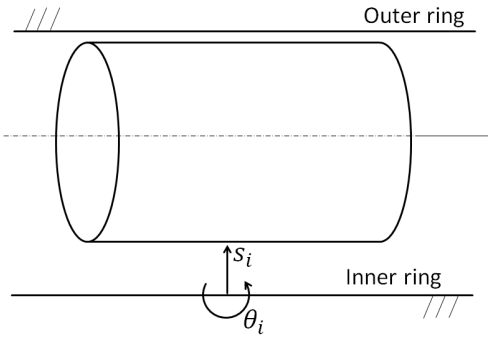

Figure 10. Roller between two raceways.

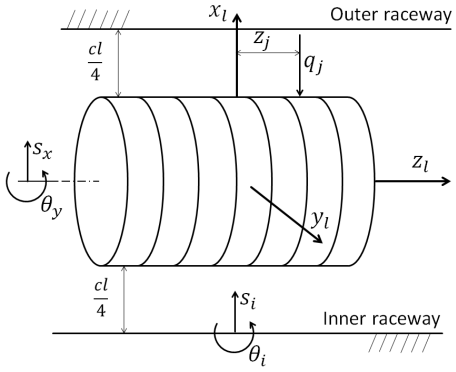

Figure 11. Sliced roller with reference parameters and local coordinate system.

The procedure to compute the model and to account for all the rolling elements is based on what developed for ACBB. As mentioned above, due to the contact load distribution along the contact line, the local wrench vector has to contain two components: the statically equivalent force ${}^lF_x$ and the statically equivalent moment ${}^lM_y$ both referred to the reference point.

Global to Local Displacements The local inner ring displacement can be defined as follows:

$$s_i = \delta_x \cos\psi + \delta_y \sin\psi, \qquad \theta_i = \mathbf{R}_{gl}^T(2,...) \begin{bmatrix} \gamma_x & \gamma_y & 0 \end{bmatrix}^T. \tag{12}$$

Where $\mathbf{R}_{gl}^T(2,...)$ indicates the second row of $\mathbf{R}_{gl}^T$. Moreover can be noticed how the axial inner ring displacement is not accounted for.

From Local to Global Loads The procedure to calculate the contribution of each rolling element to the global bearing behavior is exactly the same as described for ACBB, the only difference is in the local wrench vector which in this case is composed by two components:

$${}^j\boldsymbol{w} = \begin{bmatrix} {}^jF_x & 0 & 0 & 0 & {}^jM_y & 0 \end{bmatrix}^T. \tag{13}$$

3.1 Rolling Element Equilibrium in EHL field

In general, the rolling element does not have a cylindrical shape but micro-geometry corrections are most of the times introduced in order to reduce stress concentrations at cylinder edges and to avoid edge contact. For this purpose a certain amount of crowning is usually applied. It is introduced by the use of the formula developed by Fujiwara [12]. The crown drop at each slice location will be referred to as $\boldsymbol{\zeta}$.

The penetration between the rolling element and the raceways, in general is variable along the contacting line, due to both misalignment and crowning. In order to consider non constant penetrations the roller is sliced up as shown in Figure 11. On each slice the penetration is considered constant and it is calculated in his mean plane. The used slicing technique is based on the work done by Teutsch [13] although the proposed technique for coupling between slices will not be used. Hence each slice will not influence and will not be influenced by the neighboring slices.

The position of each slice along the roller axis, is defined by the parameter $\boldsymbol{z}_j$ which represents the distance between the roller mean plane and the mean plane of the j-th slice. Figure 11 shows the definition of the roller initial position. Figure 11 also shows the contact force acting between the raceway and the j-th slice, which is called $q_{i,j}$ or $q_{o,j}$ depending from which contact is referred to. The m slices are supposed to be short, of length l.

Roller-Outer Raceway Penetration Introducing the vector $\boldsymbol{z} \in \mathbb{R}^m$ which collects the z_l-coordinates of the mean planes of the slices, the penetration can be divided in two contributions: a constant one which considers the translation of the rolling element and a linear function which describes the rotation effect. Therefore, adding the clearance and crowning contributions, the penetration can be written as follows:

$$\boldsymbol{\delta}_o \;=\; s_x + \theta_y \mathbf{z} - cl/4 - \boldsymbol{\zeta}. \tag{14}$$

Roller-Inner Raceway Penetration This penetration can be defined considering $\boldsymbol{\delta}_o$ with the opposite sign, since if one slice approaches to the outer raceway it moves further away from the inner raceway of the same quantity. Then the contribute of the inner raceway movement is summed, which can be modeled as done before for the roller-outer raceway penetration. Thus the formulation reads:

$$\boldsymbol{\delta}_i \;=\; s_i + \theta_i \mathbf{z} - (s_x + \theta_y \mathbf{z}) - cl/4 - \boldsymbol{\zeta}. \tag{15}$$

3.2 EHL Line Contact Modeling

This subsection describes the model used to estimate the lubricated contact behavior. The roller is divided in several slices and for each slice the EHL contact model is applied to estimate the contact loads due to a given penetration coming from the current iteration step.

The lubricant fluid film thickness is estimated by the model proposed by Akbarzadeh and Khonsari [14]

Lubricant Fluid Film Behavior Based on the Reynolds equation, Moes [7] made an accurate function fit to predict the central film thickness in line contact:

$$H_c \;=\; \left[\left(H_{RI}^{7/3} + H_{EI}^{7/3} \right)^{3/7\ s} + \left(H_{RP}^{-7/2} + H_{EP}^{-7/2} \right)^{-2/7\ s} \right]^{s^{-1}} \;=\; \bar{h_c} U^{-1/2}. \tag{16}$$

where H_c and U are respectively the dimensionless central film thickness and velocity parameter while s is an auxiliary variable defined as:

$$s = \frac{1}{5}\left(7 + 8\exp\left(-2\,H_{EI}/H_{RI}\right)\right) \tag{17}$$

in which the four basic asymptotes relevant in EHL are described as function of the dimensionless lubricant (L) and load (M) parameter.

$$H_{RI} = 3M^{-1}, \quad H_{EI} = 2.621M^{-1/5}, \quad H_{RP} = 1.287L^{2/3}, \quad H_{EP} = 1.311M^{-1/8}L^{3/4}. \tag{18}$$

In the latter equations the subscripts refer to regimes, respectively RI as rigid-isoviscous, RP as rigid-piezoviscous, EI elastic-isoviscous and EP as elastic-piezoviscous.

Contact Solution As contact solution input the penetration is given, the corresponding contact force for each slice has to be computed, as well as his derivative with respect to the penetration.

In equilibrium, the penetration is overcome by the solid bodies deformation, while accounting for the additional surface separation due to the fluid film thickness, and while respecting the equality of the loading onto the solid and the lubricant.

Referring to Figure 12 the penetration can be written as function of fluid film thickness and roller deformation, as in Eq. (19) and Eq. (20). The body deformation is approximated by dry contact solution developed by Dinnik [13] since the pressure distribution onto the contact print is close to the dry case. The formulas have been handled in order to isolate the load from the constant part C_i or C_o

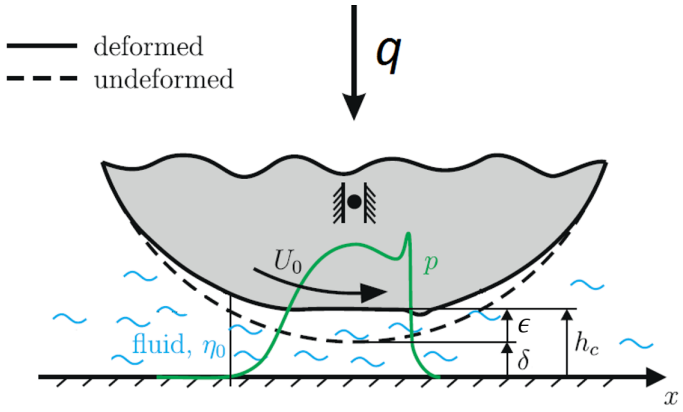

Figure 12. Contact penetration arrangement. [15]

$$\boldsymbol{\delta}_i(j) = \epsilon_{i,j} - h_{c_{i,j}} - \boldsymbol{\zeta}(j) = C_i^{-0.92}\, q_{i,j}^{0.92} - H_{c_{i,j}} U_{i,j}^{-1/2} R_{i,eq} - \boldsymbol{\zeta}(j), \tag{19}$$

$$\boldsymbol{\delta}_o(j) = \epsilon_{o,j} - h_{c_{o,j}} - \boldsymbol{\zeta}(j) = C_o^{-0.91}\, q_{i,j}^{0.91} - H_{c_{o,j}} U_{o,j}^{-1/2} R_{o,eq} - \boldsymbol{\zeta}(j). \tag{20}$$

Where the Dinnik's contact model has been introduced as well as Eq. (16). In the solution the above-mentioned equations cannot be used directly since the inverse formulation is required. Due to the complex formulation of H_c, the inverse function of Eq. (19, 20) are computed using an iterative process, thus the Newton-Raphson method is again used.

The function which has to be solved can be written starting from the definition of the penetration, for example for the slice-inner raceway contact, it reads:

$$f_{i,j}(q_{i,j}) \;=\; \epsilon_{i,j} - h_{c_{i,j}} - \boldsymbol{\delta}_i(j) - \boldsymbol{\zeta}(j) \;=\; 0. \tag{21}$$

The same can be done for the slice-outer raceway contact, defining $f_{o,j}(q_{o,j})$. To implement the iterative method the derivative of f with respect to the contact force has to be calculated:

$$\frac{\partial f_{k,j}(q_{k,j})}{\partial q_{k,j}} \;=\; \frac{\partial \epsilon_{k,j}}{\partial q_{k,j}} - \frac{\partial h_{c_{k,j}}}{\partial q_{k,j}}, \;\; k \;=\; i, o. \tag{22}$$

The terms derived form the Dinnik's formulation become:

$$\frac{\partial \epsilon_{i,j}}{\partial q_{i,j}} \;=\; 0.92\, C_i^{-0.92}\, q_{i,j}^{0.92-1}, \qquad\qquad \frac{\partial \epsilon_{o,j}}{\partial q_{o,j}} \;=\; 0.91\, C_o^{-0.91}\, q_{o,j}^{0.91-1}. \tag{23}$$

Concerning the terms $\partial h_{c_{i,j}}/\partial q_{i,j}$ and $\partial h_{c_{o,j}}/\partial q_{o,j}$, the derivative cannot be calculated manually, since $q_{k,j}$ is located also in the exponent of the exponential function. This derivative has been calculated using a symbolic tool and they are not reported here.

Finally, the iterative process can be formulated as follows:

$$q_{i,j_{k+1}} \;=\; q_{i,j_k} + \frac{f_{i,j}(q_{i,j_k})}{f'_{i,j}(q_{i,j_k})}, \;\; k = 1, \dots, \qquad q_{o,j_{k+1}} \;=\; q_{o,j_k} + \frac{f_{o,j}(q_{o,j_k})}{f'_{o,j}(q_{o,j_k})}, \;\; k = 1, \dots . \tag{24}$$

3.3 Roller Equilibrium Accounting for EHL and Centrifugal Loads

The rolling element equilibrium can be written as follows:

$$\begin{cases} F_x \;=\; \sum_{j=1}^{m} (q_{i,j} - q_{o,j}) + F_c \;=\; 0 \\ M_y \;=\; \sum_{j=1}^{m} \left[(q_{i,j} - q_{o,j})\, \mathbf{z}\,(j) \right] \;=\; 0 \end{cases} \tag{25}$$

Where F_c represents the centrifugal load acting on the roller.

In order to solve Eq. (25) an iterative process has to be employed, as usual the Newton-Raphson method is applied. The iterative process requires the definition of the Jacobian matrix, thus:

$$\mathbf{J} = \begin{bmatrix} \dfrac{\partial F_x}{\partial s_x} & \dfrac{\partial F_x}{\partial \theta_y} \\ \dfrac{\partial M_y}{\partial s_x} & \dfrac{\partial M_y}{\partial \theta_y} \end{bmatrix}. \tag{26}$$

Where the terms read:

$$\frac{\partial F_x}{\partial s_x} = \sum_{j=1}^{m} \left(\frac{\partial q_{i,j}}{\partial \boldsymbol{\delta}_i(j)} \cdot (-1) - \frac{\partial q_{o,j}}{\partial \boldsymbol{\delta}_o(j)} \cdot (1) \right), \tag{27}$$

$$\frac{\partial F_x}{\partial \theta_y} = \sum_{j=1}^{m} \left(\frac{\partial q_{i,j}}{\partial \boldsymbol{\delta}_i(j)} \cdot (-\mathbf{z}(j)) - \frac{\partial q_{o,j}}{\partial \boldsymbol{\delta}_o(j)} \cdot (\mathbf{z}(j)) \right) = \frac{\partial M_y}{\partial s_x}, \tag{28}$$

$$\frac{\partial M_y}{\partial \theta_y} = \sum_{j=1}^{m} \left[\left(\frac{\partial q_{i,j}}{\partial \boldsymbol{\delta}_i(j)} \cdot (-\mathbf{z}(j)) - \frac{\partial q_{o,j}}{\partial \boldsymbol{\delta}_o(j)} \cdot (\mathbf{z}(j)) \right) \cdot \mathbf{z}(j) \right]. \tag{29}$$

The terms $\partial q_{i,j}/\partial \boldsymbol{\delta}_i\,(j)$ and $\partial q_{o,j}/\partial \boldsymbol{\delta}_o\,(j)$ can be defined starting from Eq. (19, 20). It is sufficient to derive the penetration with respect to the load exerting on the slice and inverse it, hence:

$$\frac{\partial q_{i,j}}{\partial \boldsymbol{\delta}_i(j)} = \left(\frac{\partial \epsilon_{i,j}}{\partial q_{i,j}} - \frac{\partial h_{c_{i,j}}}{\partial q_{i,j}} \right)^{-1}, \quad \frac{\partial q_{o,j}}{\partial \boldsymbol{\delta}_o(j)} = \left(\frac{\partial \epsilon_{o,j}}{\partial q_{o,j}} - \frac{\partial h_{c_{o,j}}}{\partial q_{o,j}} \right)^{-1}. \tag{30}$$

This formulation is moreover convenient since the value of any term in the above-mentioned equations is already calculated during the processes to compute the contact forces. Therefore this calculation does not require any additional computational effort.

Once the contact stiffness is computed, the iterative process can take place using the following iterative scheme:

$$\begin{bmatrix} s_x \\ \theta_y \end{bmatrix}_{k+1} = \begin{bmatrix} s_x \\ \theta_y \end{bmatrix}_{k} - \mathrm{J}_k^{-1} \begin{bmatrix} F_r \\ F_a \end{bmatrix}_{k}. \tag{31}$$

Cylindrical Roller Bearing solution

Here the solution for a cylindrical roller bearing with the dimensions listed in Table 2 is computed. As done for ACBB a certain displacement vector is given to the inner ring with respect to the outer one. Three different rotational speed are given to the shaft, respectively $0\ rpm$, $5000\ rpm$ and $10000\ rpm$. The shaft angular position is kept as variable and the range in which it varies induces a cage rotation of $180°$, even if a minor rotation angle would be sufficient since a behavior periodicity of $360°/Z = 20°$ is expected.

The solution is computed introducing the displacements vector (32) where δ_z is not mentioned since it does not affect the solution due to the assumptions done. The values of (32) are chosen within a range that gives reasonable values of the reaction forces and moments.

$$[\delta_x \quad \delta_y \quad \gamma_x \quad \gamma_y] = \left[3 \cdot 10^{-2} mm \quad 3 \cdot 10^{-2} mm \quad 0.03° \quad 0.02°\right]. \tag{32}$$

As mentioned for ACBB, the solution shows a high shaft's speed dependency due to EHL. The modulation due to the cage rotation comes at higher frequency and lower amplitude since in this case the bearing contains a greater amount of rolling elements.

D	$5.69\ mm$	Roller diameter
L	$10\ mm$	Roller length
t	$7.16\ mm$	Outer ring thickness
$clnc$	$0.05\ mm$	Radial clearance
D_{pw}	$60\ mm$	Pitch diameter
Z	18	Number of rolling elements
E	$206\ GPa$	Young modulus
ν	0.3	Poisson ratio
ρ	$7.8\ kg/dm^3$	Material density
α_{barus}	$1 \cdot 10^{-8}\ Pa^{-1}$	Lubricant pressure-viscosity coefficient
η_0	$0.1\ Pas$	Lubricant viscosity at ambient pressure

Table 2. Estimated geometrical and material proprieties of the test bearing.

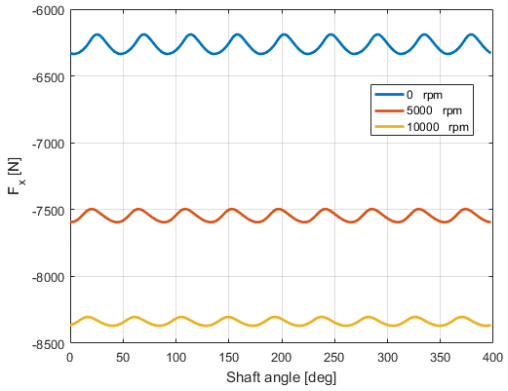

(a) Bearing reaction force along the x-axis

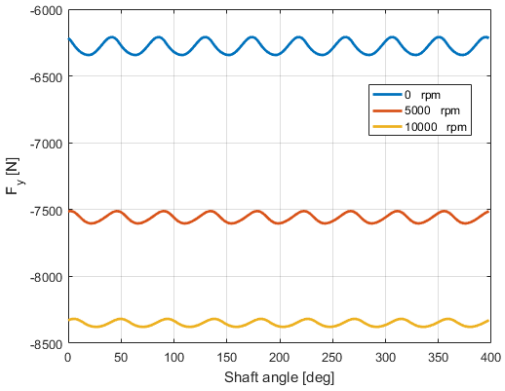

(b) Bearing reaction force along the y-axis

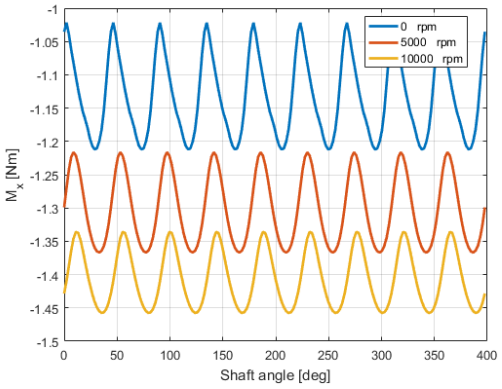

(c) Bearing reaction moment along the x-axis

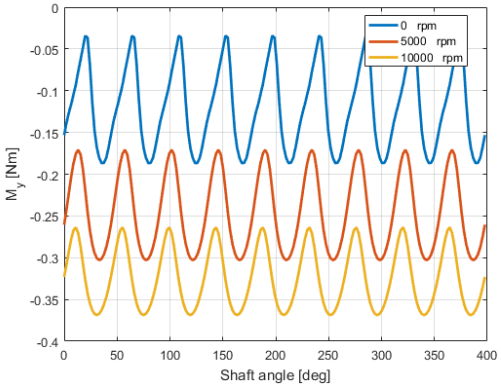

(d) Bearing reaction moment along the y-axis

Figure 13. Roller bearing reaction forces and moments assuming EHL contact

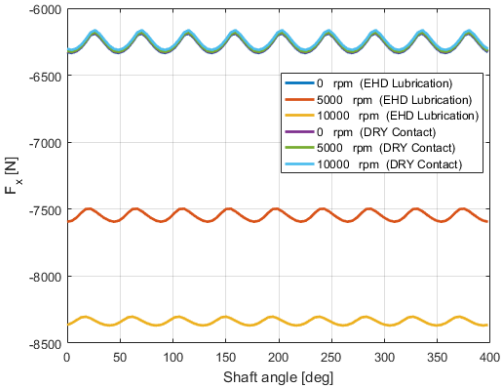

Figure 14. Comparison of the reaction force F_x calculated using EHL or Dry contact model.

Figure 14 shows a comparison between the results obtained by the here-described model and the results obtained by modeling the contact by the Hertz theory [11]. The comparison shows how in case of null rotational speed of the shaft the models return the same behavior. The difference between the results becomes non negligible as soon as the shaft rotational speed increases.

4. Conclusions

The modeling techniques in this work can calculate the steady-state behavior of a rolling element bearing by the EHL contact models. They allow for accounting of most significant phenomena by relatively easy and not time demanding computations. By the developed techniques other type of bearing can be easily analyzed by small modifications like thrust and deep groove ball bearings, tapered and barreled roller bearings. Moreover, the internal bearing behavior calculated during the solution process can be output for further post-processing.

This work sets the base for further improvements in accuracy and computation efficiency. The accuracy can be improved by more detailed contact models such as time dependent solutions which allows for the evaluation of the damping. The introduction of friction models can allow for the calculation of the slip-to-roll ratio which can affect the lubricated contact behavior and the cage speed. Another way to improve the accuracy is to account for phenomena which are not directly related to the contact, for instance the flexibility of the rings. The latter phenomena becomes particularly important in case the bearing is mounted on compliant shafts (e.g. hollow shafts) or when the bearing raceway is integrated in the gear which is quite common in planetary gear stages.

Acknowledgments The authors gratefully acknowledge VLAIO (Agency for Innovation by Science and Technology in Flanders) for the financial support through the ECOPowertrain project (Ref nr 150394) and through the Baekeland Mandate ref nr 160228 which funds the research of Leoluca Scurria.

References

[1] Staffan Andréason. Load distribution in a taper roller bearing arrangement considering misalignment. *Tribology*, 6(3):84–92, 1973.

[2] S Andreason. Theoretische grundlagen fur die berechnung von mit kraften und momenten belasteten rillenkugellagern. *Konstruktion*:105–109, 1969.

[3] JY Liu. Analysis of tapered roller bearings considering high speed and combined loading. *Journal of Lubrication Technology*, 98(4):564–572, 1976.

[4] Bernard J Hamrock and Duncan Dowson. Isothermal elastohydrodynamic lubrication of point contacts: part 1—theoretical formulation. *Journal of Lubrication Technology*, 98(2):223–228, 1976.

[5] Achi Brandt and Oren E Livne. *Multigrid techniques: 1984 guide with applications to fluid dynamics*, volume 67. SIAM, 2011.

[6] Ysbrand Hans Wijnant. *Contact dynamics in the field of elastohydrodynamic lubrication*. Universiteit Twente, 1998.

[7] H Moes. Optimum similarity analysis with applications to elastohydrodynamic lubrication. *Wear*, 159(1):57–66, 1992.

[8] ERM Gelinck and DJ Schipper. Calculation of stribeck curves for line contacts. *Tribology International*, 33(3):175–181, 2000.

[9] Tokio Sasaki, Haruo Mori, and Norio Okino. Fluid lubrication theory of roller bearing—part i: fluid lubrication theory for two rotating cylinders in contact. *Journal of Basic Engineering*, 84(1):166–174, 1962.

[10] JM de Mul, JM Vree, and DA Maas. Equilibrium and associated load distribution in ball and roller bearings loaded in five degrees of freedom while neglecting friction. i: general theory and application to ball bearings. *Journal of tribology*, 111:142–148, 1989.

[11] Leoluca Scurria. Development of modeling techniques for rolling element bearings, 2016.

[12] Hiroki Fujiwara and Tatsuo Kawase. Logarithmic profiles of rollers in roller bearings and optimization of the profiles. *NTN Technical Review*, 75:140–148, 2007.

[13] Roman Teutsch and Bernd Sauer. An alternative slicing technique to consider pressure concentrations in non-hertzian line contacts. *Journal of Tribology*, 126(3):436–442, 2004.

[14] S Akbarzadeh and MM Khonsari. Performance of spur gears considering surface roughness and shear thinning lubricant. *Journal of Tribology*, 130(2):021503, 2008.

[15] Benedikt Wiegert, Hartmut Hetzler, and Wolfgang Seemann. A simplified elastohydrodynamic contact model capturing the nonlinear vibration behaviour. *Tribology International*, 59:79–89, 2013.